OPEN ACCESS

University of BRISTOL

Xu, X., Wisnom, M., Hallett, S., Holden, G., & Gordon, B. (2016). Predicting Debonding and Delamination in Adhesively Bonded T-joints. In ECCM17 - 17th European Conference on Composite Materials: Munich, German, 26-30 June 2016. European Conference on Composite Materials, ECCM.

Publisher's PDF, also known as Version of record

Link to publication record in Explore Bristol Research
PDF-document

University of Bristol - Explore Bristol Research

General rights

PREDICTING DEBONDING AND DELAMINATION IN ADHESIVELY BONDED T-JOINTS

Xiaodong Xu[1], Michael R. Wisnom[1], Stephen R. Hallett[1], Gary Holden[2] and Barbara Gordon[2]

[1]Advanced Composites Centre for Innovation & Science (ACCIS), University of Bristol, University Walk, Bristol BS8 1TR, UK
Email: xiaodong.xu@bristol.ac.uk, m.wisnom@bristol.ac.uk, stephen.hallett@bristol.ac.uk,
Web Page: http://www.bristol.ac.uk/composites/
[2]BAE Systems, Miltary Air & Information, W386E, Warton Aerodrome, Preston, Lancashire PR4 1AX, UK
Email: gary.holden@baesystems.com, barbara@jonesgordon.freeserve.co.uk
Web Page: http://www.baesystems.com/en-uk/home

Keywords: adhesion, debonding, Finite element analysis (FEA), joints

Abstract
Different levels of FE modelling were conducted, in order to predict debonding and delamination in an adhesively bonded T-joint pull-off (T-pull) test. Specifically, 2D modelling was carried out to investigate the stress distribution in the T-pull specimen, so the locations where failures may potentially initiate could be identified, and the proper boundary conditions selected. 3D slice modelling was also conducted to predict failure propagation, to identify potential failure modes. The results indicate that the key failure mode is Mode I debonding at the deltoid. Furthermore, a half-width 3D T-pull model was set up to capture the failure mechanisms introduced by the free edges and the finite specimen width. The results indicate that Mode I debonding starts at the deltoid from the middle of the specimen, rather than from the free edges. This is due to the non-uniform stress distribution across the specimen width. The half-width 3D modelling result was compared with the 3D slice modelling result. The latter yields a slightly stiffer response due to more constraint, and a less conservative prediction because it assumes uniform stress distribution across the specimen width.

1. Introduction

A T-joint is a typical connection used in aircraft structures. The recent wide applications of adhesively bonded composite T-joints calls for better understanding of their behaviour. Efforts have been made to study the T-joint experimentally e.g. by Trask et al [1] and by Cui [2]. FE models of different levels of detail have been developed to predict the failure of the T-joint. For example, Hill et al [3] adopted a stress-based method to predict the failure of the T-joint under 'pull-off' load in a 2D FE model. Hélénon et al [4] developed a High Stress Concentration (HSC) method to predice the failure of the T-joint under bending load in a 3D FE model. Hélénon et al [5] also predicted the failure of the T-joint under tensile loads in a 3D FE model with cohesive interface elements. Cohesive interface elements were also used by Davies et al [6], Davies and Ankersen [7] to evaluate the failure of the T-joint used

in aerospace composite structures. The FE method based on cohesive interface elements is superior to the stress-based method, because the failure of the T-joint is often controlled by crack propagation.

In this paper, different levels of FE modelling of an adhesively bonded T-joint pull-off (T-pull) test were conducted and compared. 2D modelling was carried out to investigate the stress distribution in the T-pull specimen, and to identify the damage initiation 'Hotspots'. 3D slice modelling with cohesive interface elements was also conducted to predict crack propagation, and to identify potential failure modes. The results indicate that the key failure mode is Mode I debonding at the deltoid. Finally, a half-width 3D T-pull model with cohesive interface elements was set up to capture the failure mechanisms introduced by the free edges and the finite specimen width.

2. Test setup

The schematic of the test section is shown in Figure 1(a). Within the T-piece, the laminates are co-cured with film adhesive at about 180°C. Then the cured T-piece is connected to the skin section through paste adhesive.

The stacking sequences of the laminates in the test section are provided by BAE Systems. The layups determine the material properties of the numerical models. The test fixture is shown in Figure 1(b). The T-pull test will be carried out by BAE Systems. The test fixture determines the boundary conditions of the numerical models.
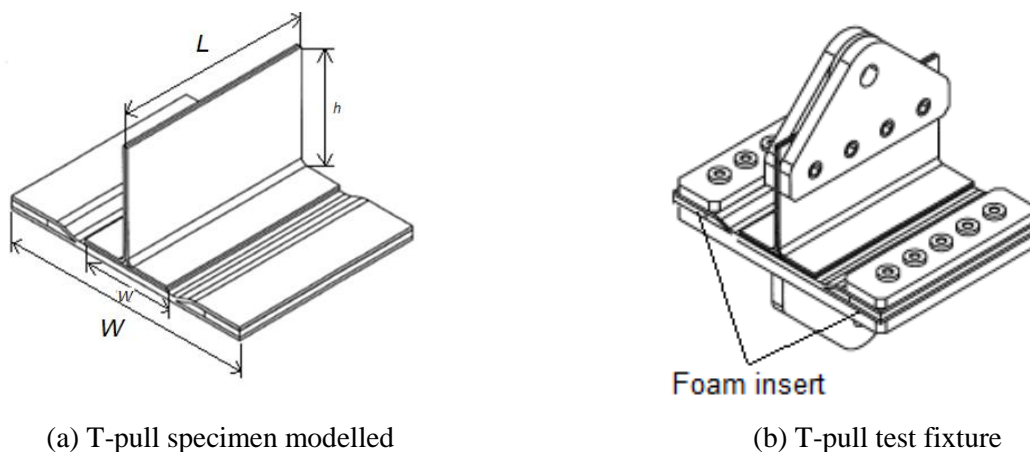

(a) T-pull specimen modelled　　　　　　　　　(b) T-pull test fixture

Figure 1. T-pull test setup.

The composite material used in the tests is IMS65/MTM44-1 UD pre-preg. In the 2D analysis, local coordinate systems are used to define the material orientations. The adhesives used in the tests are the Cytec HTA® 240/PK31 film adhesive and the Hexcel Redux® 873 paste adhesive. ROHACELL® RIMA 71 foam is inserted under the elevated skin where the steel plates are bolted as shown in Figure 1(b).

3. 2D stress analysis

The implicit FE code ABAQUS/Standard is used in the 2D analysis, in order to investigate the stress distributions in the T-pull specimen. 8-node plane-strain CPE8 elements are used in all of the 2D models. The minimum mesh size is 0.125 mm. Two elements are used through each ply, and the adhesives are not modelled (composites connected directly).

100 N/mm load, which is the typical failure load of this type of T-joint, was applied vertically at the nodes on the very top of the 2D models. A temperature drop of 160°C was applied in order to

Xiaodong Xu, Michael R. Wisnom, Stephen R. Hallett, Gary Holden and Barbara Gordon

investigate the thermal residual stresses caused by thermal contraction of the specimen from the curing temperature to room temperature. Compared with the local material coordinate systems, a global coordinate was used to define the boundary conditions as shown in Figure 2. There are two thick metal plates clamped to the top and bottom surfaces of the skin at the edges of the specimen, so all degrees of freedom of the nodes at the two surfaces were fixed, in order to simulate the clamping conditions.
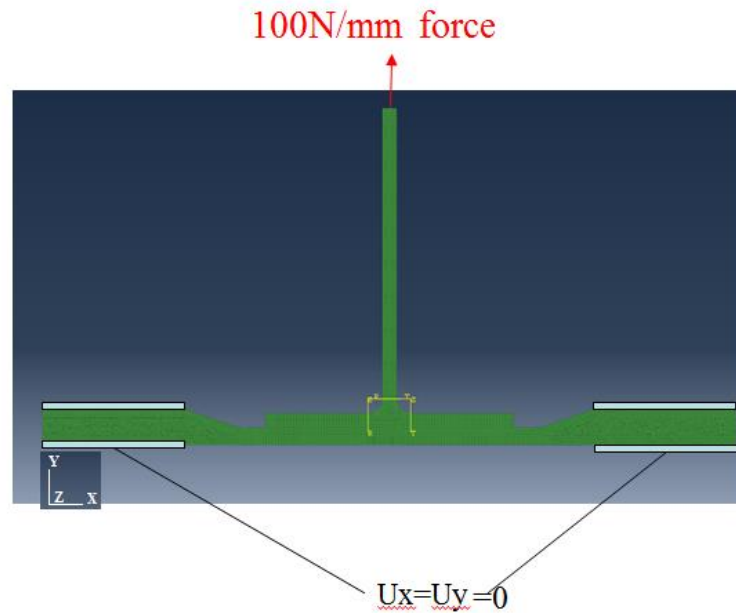

Figure 2. Boundary conditions used in 2D analysis.

The results indicate that the foam inserted between the skins near the boundaries has no effect on the stress distributions. This is because of the clamping boundary conditions and the fact that the foam is away from the deltoid. Although foam is still modelled in the 2D analysis, it will not be modelled in the 3D analysis (replaced by air), in order to reduce the number of elements.

In this 2D linear FE analysis, the 2D plane-strain models with two levels of mechanical loads (100 N/mm and 200 N/mm) are compared. The stress distributions under the other applied mechanical loads can be interpolated from these two sets of results. Equation 1 is used as the damage initiation criterion, which assumes quadratic interaction between the through-thickness tensile stress and the inter-laminar shear stress,

$$\left(\frac{S_{zz}}{S_{zz,C}}\right)^2 + \left(\frac{S_{yz}}{S_{yz,C}}\right)^2 \geq 1 \qquad (1)$$

where, $S_{zz,C}$, and $S_{yz,C}$ are the inter-laminar tensile and shear strengths of the material.

The resultant stresses, which are the summation of the thermal residual stresses and the stresses under mechanical loads are checked. The stress increments per unit load can be calculated.

The hotspots where debonding and delamination can potentially initiate are identified in a schematic in Figure 3. They are the top of the deltoid (Hotspot 1), maximum tension location at the film adhesive near the deltoid (Hotspot 2), maximum shear location at the film adhesive near the deltoid (Hotspot 3) and the stringer foot between the T-piece and the skin (Hotspot 4). At Hotspot 4, the 2D stress analysis cannot provide accurate predictions due to the stress singularity arising at the discontinuity. Therefore further fracture analysis needs to be done in the 3D analysis.
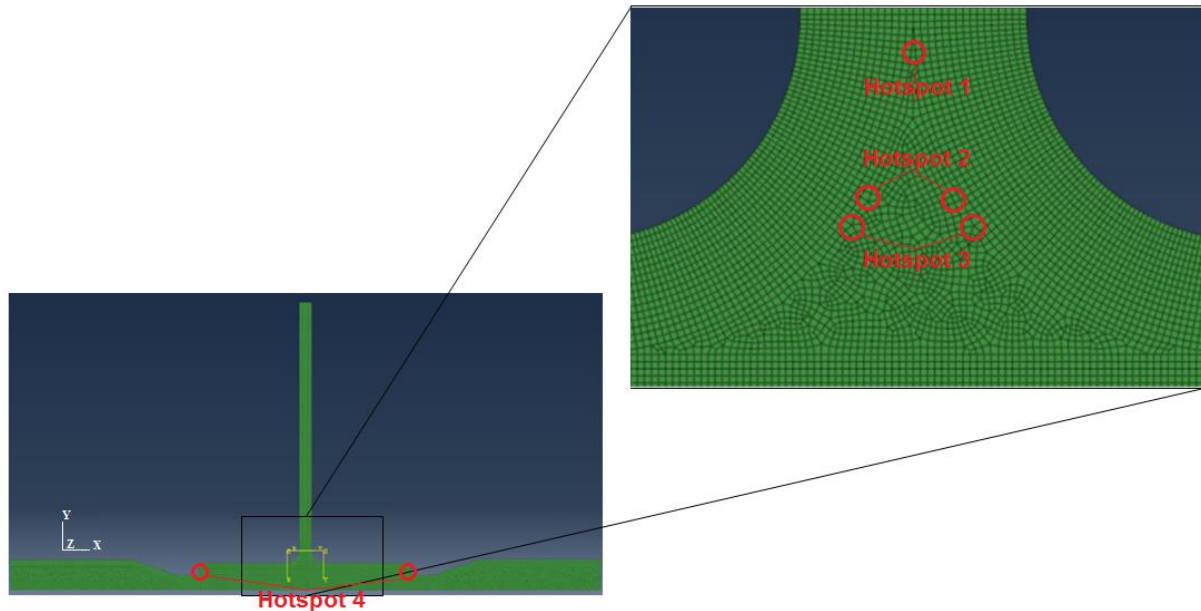
Figure 3. Identified hotspots in 2D analysis.

4. 3D slice modelling

An FE method using the explicit code LS-Dyna is applied in the 3D slice analysis, in order to predict failures in the T-pull tests. Detailed ply-by-ply 3D models with a single row of 8-node constant stress solid elements across the slice width are constructed, producing a quasi-2D model. The minimum mesh size is 0.125 mm. There is one element through each ply thickness (0.25 mm). The 3D slice model is 0.125 mm wide with one element across its width.

Displacements are applied vertically at the nodes on the very top of the 3D slice models. A temperature drop of 160°C is also applied to the models. The boundary conditions in the 2D analysis are applied to the 3D slice models. Additionally, all the nodes at the front and back faces are fixed in the width direction to simulate a plane-strain stress state.

In the 3D slice analysis, cohesive interface elements are used to simulate the potential debonding at the adhesives and the potential delamination between every pair of adjacent laminate plies. A mixed-mode traction-separation law [8] is applied in the cohesive interface elements. There are two criteria. One is a stress-based criterion for damage initiation, which assumes quadratic interaction between the through-thickness tensile stress and inter-laminar shear stress. The other one is an energy-based criterion for full debonding, which assumes linear interaction between the Model I strain energy release rate and the Mode II strain energy release rate. High modulus values (1000 GPa) are used for the cohesive elements which have a thickness of 0.01 mm.

The baseline 3D slice modelling predictions are shown in Figure 4. The grey lines are the pre-defined potential debonding and delamination paths. The damaged cohesive interface elements in which the stress-based initiation criterion is met are marked in green. The fully failed cohesive interface elements in which the critical strain energy release rate has been exceeded are marked in red, corresponding to debonding and delamination. The noise on the load-displacement curves is caused by the dynamic effects introduced by mass scaling in the quasi-static explicit FE analysis.
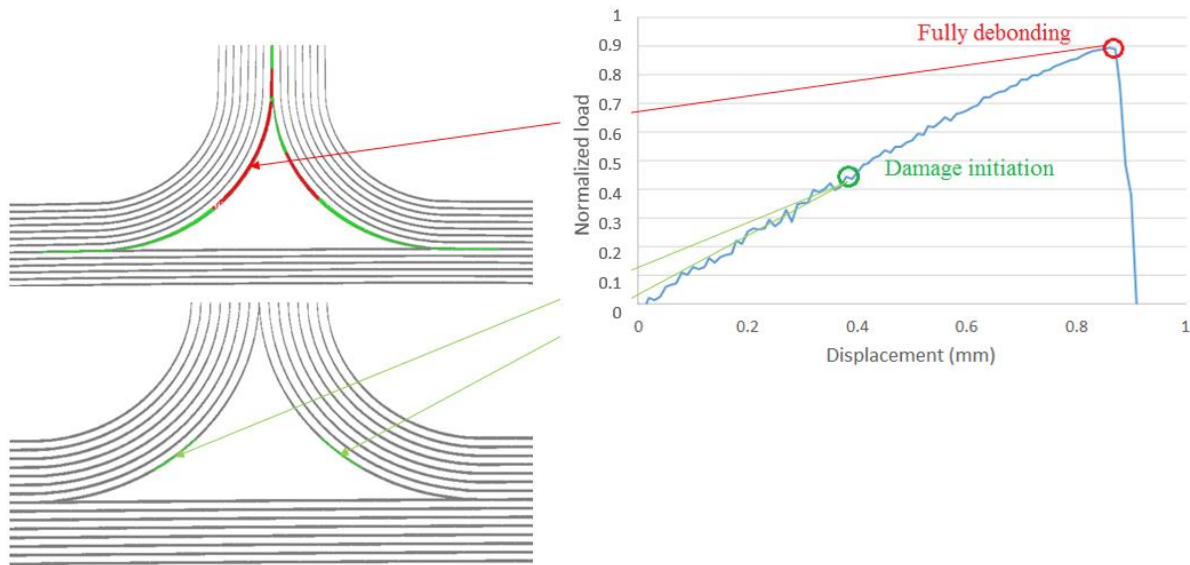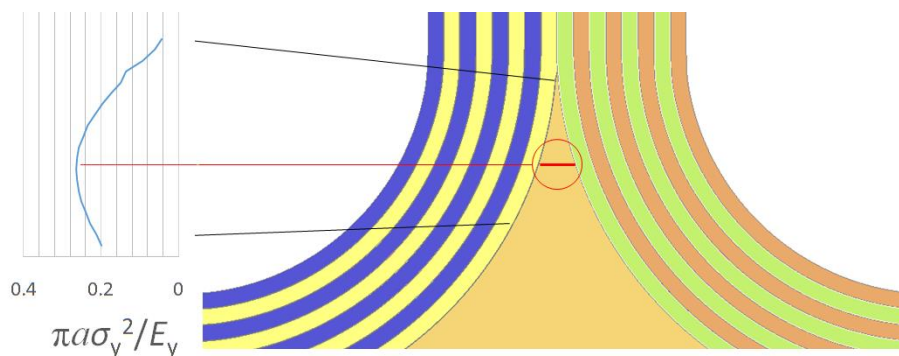
Xiaodong Xu, Michael R. Wisnom, Stephen R. Hallett, Gary Holden and Barbara Gordon

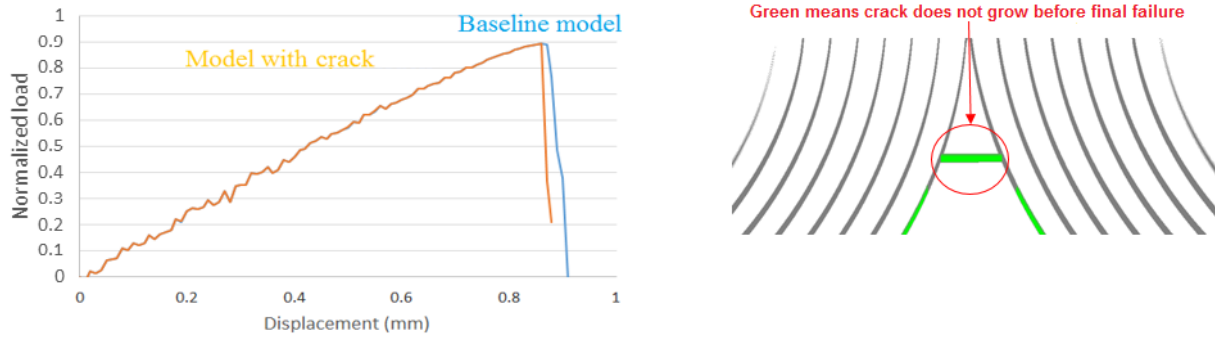**Figure 4**. 3D slice model predicts failure at the film adhesive.

From the load-displacement curve on the right and the damage plots on the left, the baseline 3D slice model predicts that the damage initiates within the film adhesive near the deltoid. However, after damage initiates, the T-pull model does not fail immediately, but keeps withstanding load until the film adhesive at the deltoid fully debonds.

The 3D slice model also predicts that the damage initiates within the paste adhesive at the stringer foot between the T-piece and the skin even under thermal loads. However, such damage never propagates. In order to predict debonding at the paste adhesive, the failure of the film adhesive and laminates were prohibited. It takes 44% higher load to debond the paste adhesive than the load needed to debond the film adhesive.

A crack path was additionally pre-defined with a line of cohesive interface elements at the top of the deltoid in the 3D slice model, in order to simulate a delamination that might be generated under thermal loads. The worst location for such a crack is not obvious. On the one hand, at the very top of the deltoid, the stress is high but the crack length is zero (the available strain energy is zero). On the other hand, lower down the deltoid, the crack is long, but the stress level is low (the available strain energy is also low). The strain energy release rate needed to drive such a crack to propagate is proportional to crack length times stress squared. This is plotted against the vertical position at the top of the detoid. A line of elements are therefore chosen at approximately the worst location for the crack to grow along the interface as shown in Figure 5(a). Although the crack initiates under thermal loads according to the FE results in Figure 5(b), it does not migrate into the film adhesive before final failure. Therefore, it has no effect on the expected failure loads.

$$\pi a \sigma_y^2 / E_y$$

(a) Crack at the top of the deltoid

Xiaodong Xu, Michael R. Wisnom, Stephen R. Hallett, Gary Holden and Barbara Gordon

(b) Prediction with thermal crack in deltoid
Figure 5. Crack at the top of the deltoid.

5. Half-width 3D modelling of the T-pull tests

The same FE method using the explicit code LS-Dyna with cohesive interface elements is applied in the half-width 3D modelling of the T-pull tests. Efforts are made to reduce the number of elements. In particular, the cohesive elements away from the 'Hotspots' are removed. The minimum mesh size is 0.125 mm. There is one element through each ply thickness (0.25 mm). The half-width 3D T-pull model has a refined mesh (0.25 mm) at the free edge across the width, in order to capture the potential free edge effects. A coarser mesh is used away from the free edge across the width.

Similar boundary conditions to those used in the 3D slice analysis are applied to the half-width 3D model. Displacements are applied to the nodes at the very top of the model. Although the nodes at the symmetry plane are fixed in the width direction, the nodes at the free edge are left unconstrained.

The FE results indicate the vertical displacement distribution is not uniform across the model width, as shown in Figure 6. This is due to the anticlastic curvature. The effect is made more pronounced by the very high Poisson's ratio of the angle plies on the top surface and the mismatch of properties between laminates.
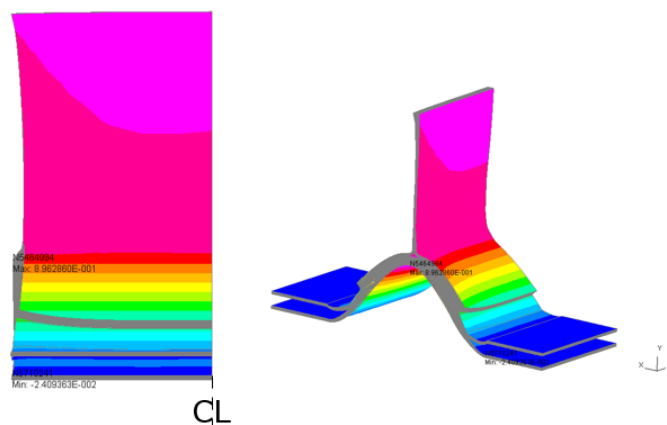

Figure 6. Non-uniform displacement distribution across the model width (mm).

Such strong 3D effects also result in the non-uniform vertical stress distribution within the stringer web across the model width, as shown in Figure 7. The vertical stresses are higher near the symmetry plane of the model, and drop significantly when approaching the free edge. Near the free edge, the vertical stresses increase again due to the singularity at the free edge. However, the vertical stress distribution is less non-uniform across the width closer to the top of the deltoid, which implies that the actual load distribution at the deltoid is more uniform than might appear from looking at the displacements.
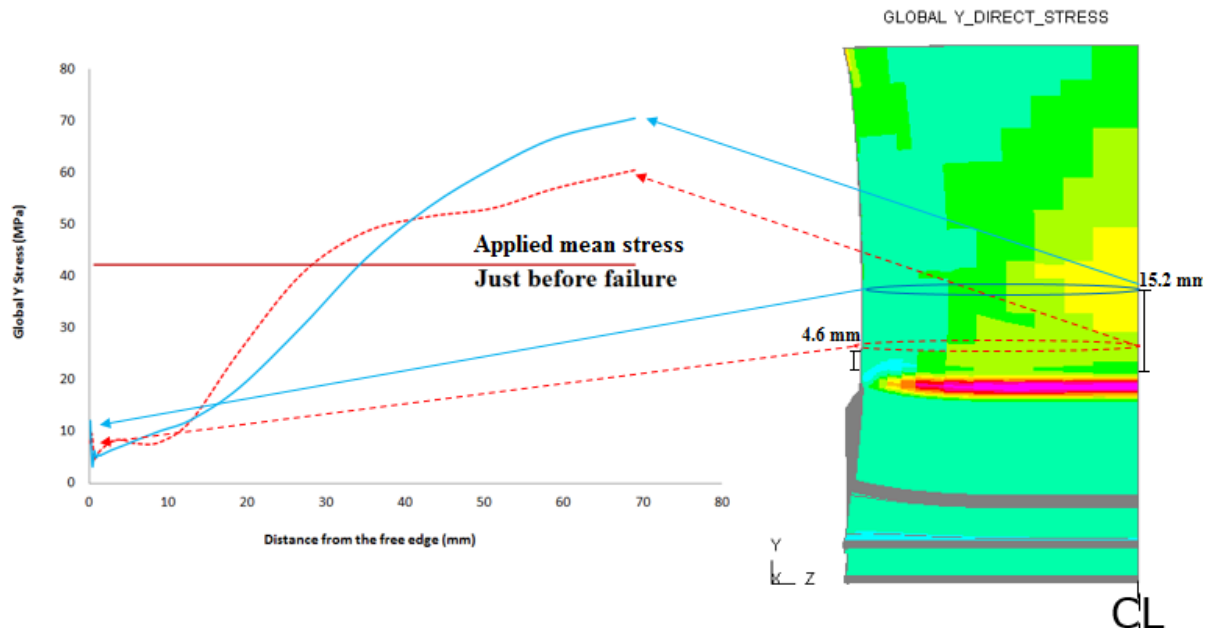
Xiaodong Xu, Michael R. Wisnom, Stephen R. Hallett, Gary Holden and Barbara Gordon

Figure 7. Non-uniform vertical stress distribution across the width (MPa).

The half-width 3D model of the T-pull tests predicts that damage initiates (in green) and propagates (in red) from the symmetry plane of the model, rather than from the free edge, as shown in Figure 8. This is due to the non-uniform stress distribution across the model width with a higher level of stresses in the middle.
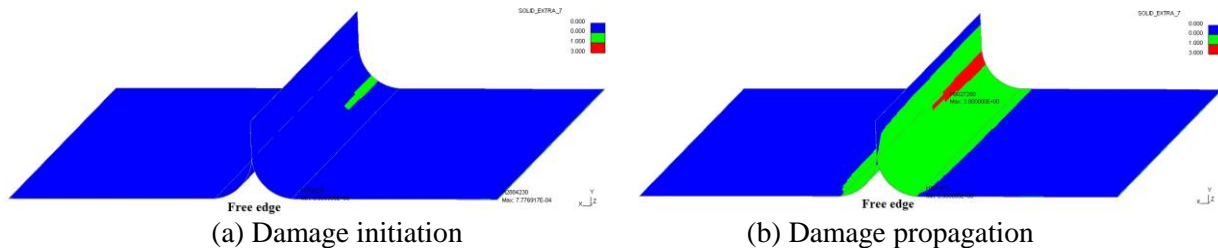

(a) Damage initiation   (b) Damage propagation

Figure 8. Damage development in the half-width 3D T-pull model.

The half-width 3D modelling predicts that damage at the film adhesive propagates from the centre line, so an additional case was run with reversed mesh (fine mesh near the centre line rather than at the free edge) and the results were found not to be sensitive to the two different mesh arrangements.

In summary, the predictions for damage initiation between models of different levels of detail are within 11%. More importantly, the predictions for damage propagation (final failure) between the 3D slice model and the 3D half-width are within 6%. The slice modelling predicts a stiffer response than the half-width model 3D model due to the higher constraint across the specimen width preventing anti-clastic bending. It predicts a slightly stronger response than the half-width 3D model. This is due to the non-uniform stress distribution across the width in the half-width 3D model, although the effect is not large as the stress distribution is less non-uniform right at the top of the deltoid.

6. Conclusions

The 2D analysis implies that damage may initiate within the laminate at the top of the deltoid under thermal loads (Hotspot 1). However, at Hotspot 1, the crack may not propagate due to constraint from

the adjacent laminates, which is confirmed by the 3D slice modelling results. The 2D analysis also suggests that debonding may initiate within the film adhesive near the deltoid at Hotspot 3 (location of maximum shear).

The 3D slice models behave reasonably well, and can be used for comparative studies when computational capacity is limited. The T-pull slice modelling shows that the key failure mode is Mode I dominated debonding at the film adhesive at the deltoid. The T-pull slice analysis indicates that the crack at the top of the deltoid (Hotspot 1), and that at the stringer foot (Hotspot 4) initiate under thermal loads, but do not propagate, so do not affect the ultimate failure of the specimen. It takes 44% higher load to debond the paste adhesive.

The half-width 3D model with refined mesh at the free edge is very robust. The half-width 3D modelling of the T-pull tests indicates a non-uniform vertical stress distribution across the model width in the stringer web. Damage does not initiate and propagate from the free edge, but from the middle of the specimen at the deltoid. However, the vertical stress distribution is more uniform across the specimen width at the very top of the deltoid, making the slice models still a reasonable prediction tool.

Acknowledgments

References

[1] R. S. Trask, S. R. Hallett, F. M. M. Helenon, and M. R. Wisnom, Influence of process induced defects on the failure of composite T-joint specimens, *Composites Part A: Applied Science and Manufacturing,* 43:748-757, 2012.

[2] H. Cui, *Delamination and debonding failure of laminated composite T-joints*, PhD thesis, Department of Aerospace Structures and Materials, TU Delft, The Netherlands, 2013.

[3] F. J. G. Hill, M. R. Wisnom, and M. Jones, Failure Prediction of Composite T-Piece Specimens, *Proceedings of the ICDFC5 conference, London, UK,* 1999.

[4] F. Hélénon, M. R. Wisnom, S. R. Hallett, and R. S. Trask, Investigation into failure of laminated composite T-piece specimens under bending loading, *Composites Part A: Applied Science and Manufacturing,* 54:182-189, 2013.

[5] F. Hélénon, M. R. Wisnom, S. R. Hallett, and R. S. Trask, Numerical investigation into failure of laminated composite T-piece specimens under tensile loading, *Composites Part A: Applied Science and Manufacturing,* 43:1017-1027, 2012.

[6] G. A. O. Davies, D. Hitchings, and J. Ankersen, Predicting delamination and debonding in modern aerospace composite structures, *Composites Science and Technology,* 66:846-854, 2006.

[7] G. A. O. Davies and J. Ankersen, Virtual testing of realistic aerospace composite structures, *Journal of Materials Science,* 43:6586-6592, 2008.

[8] W.-G. Jiang, S. R. Hallett, B. G. Green, and M. R. Wisnom, A concise interface constitutive law for analysis of delamination and splitting in composite materials and its application to scaled notched tensile specimens, *International Journal for Numerical Methods in Engineering,* 69:1982-1995, 2007.

Xiaodong Xu, Michael R. Wisnom, Stephen R. Hallett, Gary Holden and Barbara Gordon